Influence of Interface on the Charge Carrier Mobility of La2Ti2O7 Layered Perovskite Thin Films Measured by the Time-of-Flight Method

Sébastien Leroy, Redouane Douali, Christian Legrand, Freddy Krasinski, Florent Blanchard, Pascal Roussel, S. Saitzek, Jean-François Blach

Influence of interface on the charge carrier mobility of $La_2Ti_2O_7$ layered-perovskite thin films measured by time of flight method

Sébastien Leroy[1], Redouane Douali[2], Christian Legrand[2], Freddy Krasinski[2], Florent Blanchard[3], Pascal Roussel[3], Sébastien Saitzek[1], Jean-François Blach[1,]*

1 Univ. Artois, CNRS, Centrale Lille, Univ. Lille, UMR 8181, Unité de Catalyse et Chimie du Solide (UCCS), F-62300 Lens, France

2 ULCO, Unité de Dynamique et Structure des Matériaux Moléculaires (UDSMM) EA 4476, F-62100 Calais, France

3 Univ. Lille, CNRS, Centrale Lille, Univ. Artois, UMR 8181, Unité de Catalyse et Chimie du Solide (UCCS), F-59000 Lille, France

ABSTRACT

We report the electrical characterizations of $La_2Ti_2O_7$ thin films synthetized by pulsed laser deposition. We observe a significant change in I-V curve in the presence of UV light. The conduction mechanism can be described by two regimes: ohmic at low voltage and space charge limited conduction for higher voltage. Finally, for the first time to our knowledge, the charge carrier mobility of this material is studied; we use the time of flight method to investigate this property. We explain the evolution of the carrier mobility with the applied voltage by the presence of a depletion layer between the film and the gold contact which affects the measurements.

TOC GRAPHIC

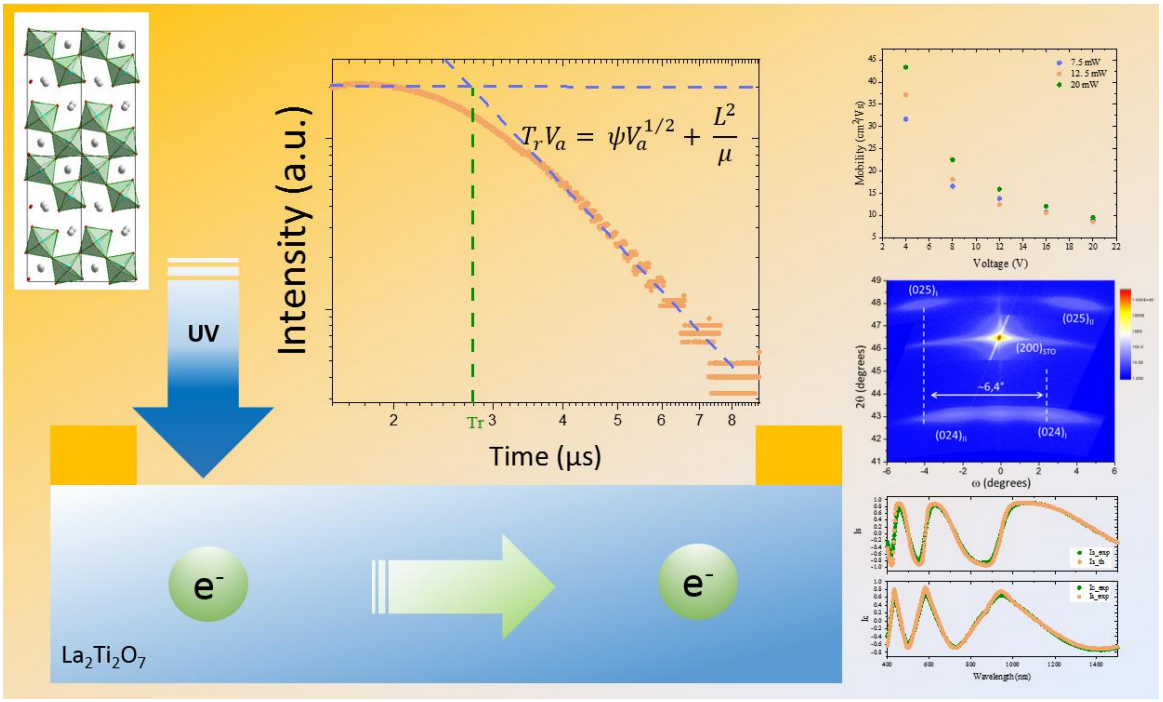

KEYWORDS : $La_2Ti_2O_7$, thin films, perovskites, time of flight, carrier mobility

INTRODUCTION

Oxide materials have been extensively studied these last years for many applications as ferroelectric memories, piezoelectric actuators[1], solar cells[2], batteries[3], luminescence[4] … Among them, layered perovskites and especially, rare earth titanates with chemical formula $Ln_2Ti_2O_7$ reveal interesting properties. Particularly, Lanthanum dititanate, $La_2Ti_2O_7$ (hereafter LTO) was widely studied. At room temperature $La_2Ti_2O_7$ crystallizes in a monoclinic structure with space group $P2_1$, and possesses a layered structure formed by infinite layers of TiO_6 octahedra. This oxide is ferroelectric in a large range of temperature[5], has a high dielectric constant, and can be used as heterojunction for photocatalytic applications[6,7], electrode material[8]. In addition, in recent years numerous research activities concerning the design of all-oxide solar cells[9] have been conducted, the main interest of those compounds being its non-toxicity and an easily recyclability. For these applications, the control of electronic properties is important to improve their performances. In this context, many publications[10,11] present ab-initio calculation of the band structure of these $Ln_2Ti_2O_7$ oxides. These calculations are fundamental for applications, especially for the determination of the band structure and optical band-gap which gives the range of wavelength for electronic absorption or an estimation of the physical properties such as the conductivity. But, despite of this large amount of publications, there is, to our knowledge, no experimental articles presenting experimental measurements of the charge carrier mobility of rare earth titanates and particularly of the Lanthanum dititanate. The determination of the charge carrier mobility can be achieve using two technics: (i) Space-charge-limited current measurements [12–14]; in this case the material, usually a thin film, is connected to a metal electrode by an ohmic contact. This electrode injects the charge carriers into the material and the drift time is measured with a second electrode. (ii) Time of flight (TOF) measurements [15–17]; in this

measurement the charge carriers injection is produced by light. Photo-carriers are created by light pulses between two electrodes and an electric field induces a photocurrent.

In this article we present an experimental study of the charge carrier mobility of $La_2Ti_2O_7$ thin film. In a first part we will detail the preparation of the target and the synthesis of the thin films, as well as their structural characterization. The second part is devoted to the measurements of I-V curves. The last part will describe the results obtained by TOF measurements.

RESULTS AND DISCUSSION

Figure 1.a presents the XRD pattern of $La_2Ti_2O_7$ films grown on (100)-oriented $SrTiO_3$ substrate for various oxygen pressure and for substrate temperature fixed at 950°C. First of all, an oxygen pressure greater than 10^{-3} mbar is necessary to obtain the $La_2Ti_2O_7$ phase with the reflections of the planes (012) and (025). This particular growth has already been observed in a previous work on the growth of $La_2Ti_2O_7$ films by sol-gel associated with the spin-coating technique[18]. At the end of the deposition, 200 mbar of oxygen are introduced in order to promote the $La_2Ti_2O_7$ phase and limit the formation of Ti^{3+} [19,20]. For lower pressures (i.e. 10^{-5} mbar) and without adding oxygen at the end of deposition, the diffraction peaks can be indexed according to the (*h00*) orientation of the $LaTiO_{3+\delta}$ pseudo-cubic phase [19]. We can also note that a minimum temperature of 900°C is required to obtain the oriented $La_2Ti_2O_7$ films.

In order to better understand the adaptation of the two structures, we continued our investigations by carrying out rocking-curves on the (012) reflection. We observe that, depending on the φ

angle (i.e. on the orientation of the film in the diffractometer), the rocking-curve either presents two or three peaks. By plotting the evolution of these rocking-curves as a function of φ, we clearly observe a periodicity on the 2D intensity map (figure 1.b). As discussed in detail in our previous work [18], this result indicates the presence of four equivalent domains inclined of 1.6° relatively to the plane of the substrate (a model explaining the presence of these 4 domains is proposed in figure S1 - Supporting information). These four domains can be induced by the iso-probability of growth in both spatial directions (0° and 90°) of cubic $SrTiO_3$ substrate and by the presence of a twinned structure within the structure of $La_2Ti_2O_7$. Indeed, H. W. Schmalle et *al.* [21] describes that the LTO crystals are systematically twinned and the twinning operator is a mirror perpendicular to the c* axis. We can also note that $La_2Ti_2O_7$ behaves isostructurally to $Nd_2Ti_2O_7$ described in our previous works [22].

In addition, we recorded a pole figure to verify if the layer was textured or epitaxial. For this, we have chosen an angle $2\theta = 33.01°$ (Figure 2.a). This angle was chosen to observe on the same figure both poles of the substrate and the most intense reflections of the $La_2Ti_2O_7$ phase. We observe several reflections that were indexed using the STEROPOLE software [23] considering the epitaxial orientation relationships as $[010]_{STO}/[01\text{-}2]_{LTO}$ (tilted ~1.6°), $[100]_{STO}//[012]_{LTO}$ (tilted ~1.6°) and $[001]_{STO}//[100]_{LTO}$ (tilted ~1.6°). However, full indexing can be achieved only by considering the 4 variants (denoted I, II, III and IV) as indicated in the model of Figure S1 – Supporting information. This interpretation leads to an epitaxial growth along the direction (012) slightly inclined by 1.6 ° but does not explain the presence of the (025) reflection. We therefore continued our investigations by mapping the reciprocal space around the (200) node of the substrate (figure 2.b). On this map, we can distinguish several nodes that can be indexed with the (012) and (025) reflections inclined with respect to the substrate plane. These two reflections are

part of the same crystallite. Indeed, the angle between the planes (024) and (025) is 6.37° (Figure S2.a – Supporting information).

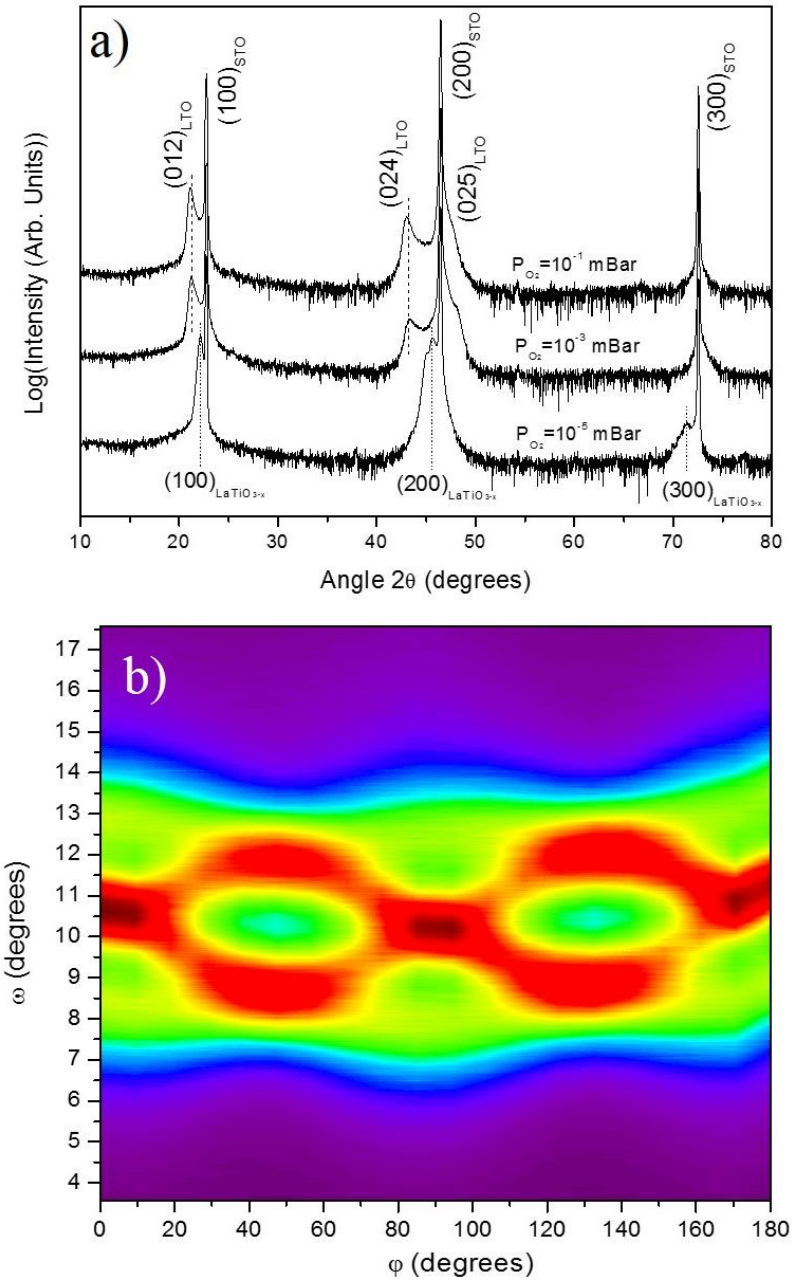

Figure 1. a) Influence of oxygen pressure on XRD patterns of $La_2Ti_2O_7$ thin films grown on (100)-oriented $SrTiO_3$ substrate ($T_{substrate}$=950°C) ; b) 2D map representation of the rocking-curve *vs.* φ angle.

Moreover, the presence of twinning explains the observed symmetry and the presence of the equivalent poles indexed I and II in Figure 2.b. The adaptation of the two structures (presented in Figure S2.b – Supporting information) reveals a stacking defect every two blocks made up of 4 octahedron sheets of TiO_6, probably explaining the angle of inclination observed. Consequently, this structural arrangement has an iso-probability of deposition in both directions of space but can also be reversed (twinning) thus inducing 4 arrangement possibilities and hence the four domains observed in the pole figure.

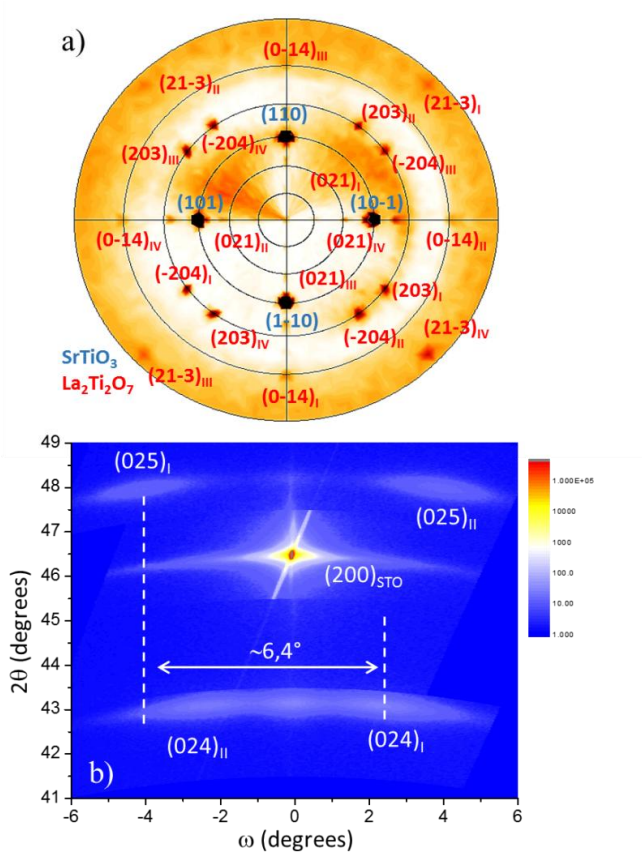

Figure 2. (a) Pole figure performed at 2θ = 33.01° on $La_2Ti_2O_7$ thin film grown on (100)-$SrTiO_3$ (the indexations in blue correspond to the positions calculated for the $SrTiO_3$ substrate while the indexations in red correspond to the $La_2Ti_2O_7$ poles); (b) Reciprocal Space Map carried out around $(200)_{STO}$ node at φ = 0° for $La_2Ti_2O_7$/(100) -$SrTiO_3$ thin film elaborated at 950°C under a pressure of 10^{-3} mbar.

Regarding the deposition on the Pt-(111)/TiO_x/Si substrates (Neyco supplier), we first determined the thermal stability of the substrate by carrying out various anneals at atmospheric pressure. From 600°C, we can see that the Pt electrode reacts with the substrate to form PtSi compound. For the growth of $La_2Ti_2O_7$, we thus limited our substrate temperature to 500°C. However, the XRD pattern realized in conventional parallel beam does not indicate any reflection of the

presence of an amorphous or polycrystalline layer (the reflections of the film being obscured by the strong intensities of the reflections of the substrate). To obtain information related to the deposited film, we performed a µXRD measurement (400 µm spot) without monochromator by slightly shifting from the normal of the substrate. The µXRD pattern is shown in Figure 3. Thanks to this technique, we were able to observe the characteristic reflections of the $La_2Ti_2O_7$ phase. The asterisk indicates the presence of a TiO_x phase (platinum bond layer on silicon). In conclusion, for the deposits on Pt-(111)/TiO_x/Si, we therefore obtain a polycrystalline layer of $La_2Ti_2O_7$. In addition, a preferential orientation is also observed along the (004) plane.

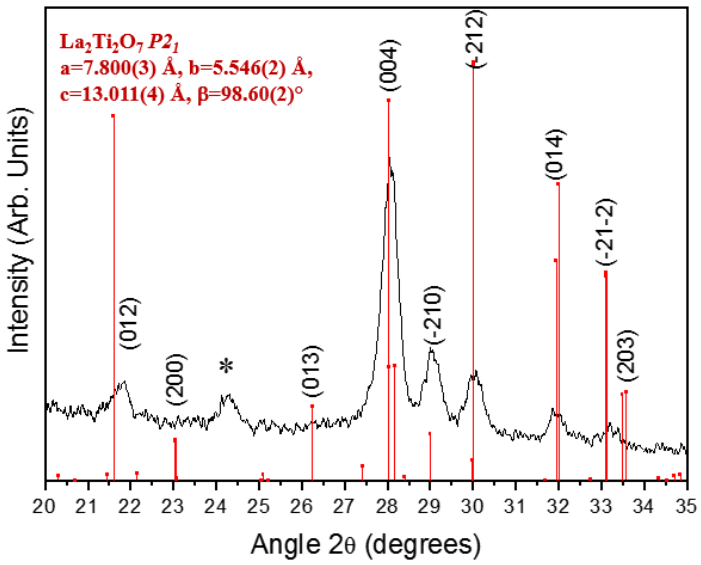

Figure 3. µXRD pattern of $La_2Ti_2O_7$ thin film grown on Pt-(111)/TiO_x/Si substrate.

Spectroscopic ellipsometry measurements were carried out for the nondestructive determination of the thickness and the optical properties of $La_2Ti_2O_7$ thin films. All measurements were performed using an incidence angle of 70°. Then, the modeled files containing the Is (λ) and Ic

(λ) signals were compared to the values obtained from the experiment. This model consists to create a stacking of layers with the same optical properties than the original sample ($La_2Ti_2O_7/SrTiO_3$ or $La_2Ti_2O_7/Pt/TiO_x/Si$). The optical functions of the platinum layers, TiO_x Layer, $SrTiO_3$ substrate, silicon substrate can be found in the database of Horiba Delta-Psi 2 software. Concerning the optical function of $La_2Ti_2O_7$, we use the procedure described on a previous article [24]. The main idea consists to perform a fitting process in the transparency region of $La_2Ti_2O_7$ with a transparent Cauchy optical function in order to obtained the thickness. And in a second step, when the thickness is fixed, it is possible to extract directly the optical function in the whole experimental range (300-1500 nm) and obtain the optical properties as the value of the optical band gap.

Concerning the sample $La_2Ti_2O_7/Pt/TiO_x/Si$, the thickness of the $La_2Ti_2O_7$ thin film is determined at 390 nm. In addition, the knowledge of the optical function of $La_2Ti_2O_7$ allows us the determination of its optical band gap by plotting $(\alpha E)^2$ versus E where α and E are respectively the absorption coefficient and the photon energy as $La_2Ti_2O_7$ can be considered at a n-type semiconductor [24]. We found an optical band gap Eg = 3.93 eV and one can conclude that this thin $La_2Ti_2O_7$ layer can absorb the light in the UV region (Figure 4). The same value was obtained with the sample of $La_2Ti_2O_7$ deposited on a $SrTiO_3$ substrate.

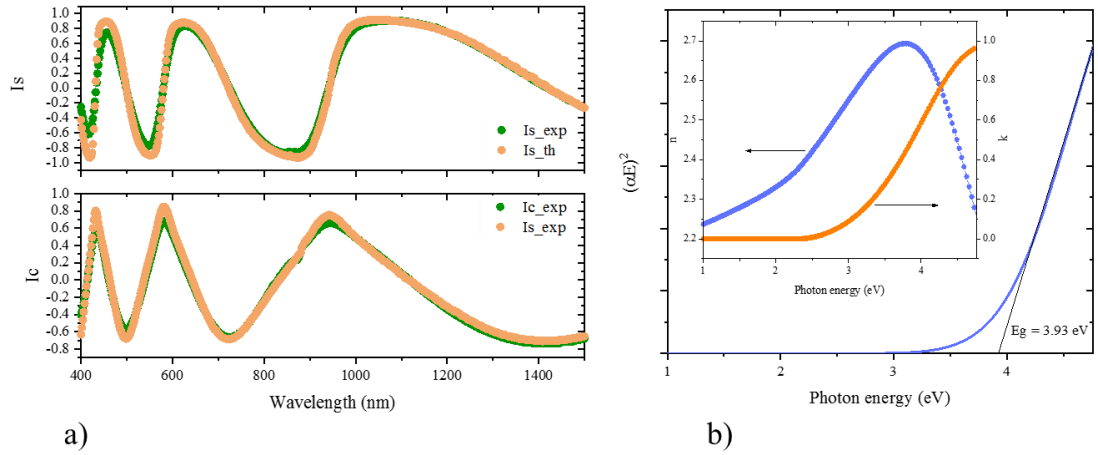

Figure 4. a) Results on Is and Ic curves for the $La_2Ti_2O_7$ film (modeled by the Cauchy relation) deposited on /Pt/TiO_x/Si substrate. The green and orange curves represent the experimental and calculated data, respectively. b) Tauc plot of $La_2Ti_2O_7$ thin films (inset: refractive index and extinction coefficient of $La_2Ti_2O_7$ versus photon energy)

Electrical characterizations were performed on the $La_2Ti_2O_7$ layer to investigate the electrical behavior of this thin film with the application of a UV light. On one side, $La_2Ti_2O_7$/Pt/TiO_x/Si sample covered by gold electrodes was used for the measurements of current-voltage curves. On the other side, for the Time of Flight measurements, to avoid leakage of photo-generated charge carriers in the back platinum electrode we used the $La_2Ti_2O_7/SrTiO_3$ sample covered by gold electrodes (planar geometry). In addition, with this $La_2Ti_2O_7/SrTiO_3$ sample we can also irradiate easily the $La_2Ti_2O_7$ layer between the two top electrodes and observe the photocurrent.

Forward and reverse bias current-voltage characteristics were measured on the $La_2Ti_2O_7$ thin film deposited on a Silicon substrate covered by a platinum electrode. Top gold electrodes of 0.09 mm^2 surface area were deposited on the $La_2Ti_2O_7$ thin film to perform the electrical measurements. The measurements were performed in the dark and under UV illumination at 365

nm in order to observe as expected previously a photocurrent. The results are depicted on Figure 5 (a) on a semi-logarithmic graph.

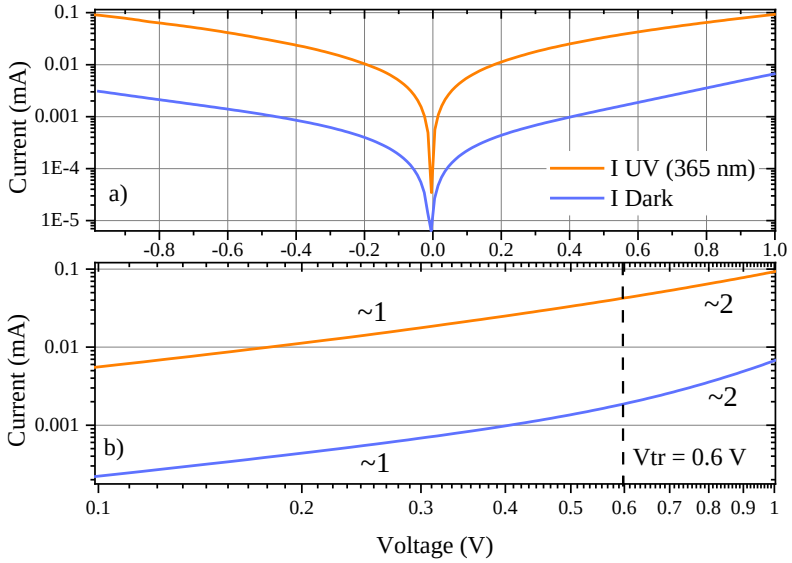

Figure 5. Forward and reverse bias current-voltage characteristics of $La_2Ti_2O_7$ thin film obtained in the dark (blue curve) and under UV light (365 nm, orange curve) : a) in semi-logarithmic graph b) in log-log graph.

Firstly, note that the I-V curve obtained for the sample in the dark can indicates the Schottky nature of the diode[25]. Secondly, a significant increase of the current occurs for both bias when the sample is illuminated by the UV light. Such an evolution was already observed for instance in $Pb_{0.6}Li_{0.2}Bi_{0.2}Zr_{0.2}Ti_{0.8}O_3$ (PLBZT) ceramics [26] illuminated under white light. This increase of the current is due to photo-generated charge carriers which gain enough energy under UV light to jump from valence band to conduction band and can cross the Schottky barrier at the thin film / electrode interface. This significant photocurrent can be potentially very interesting, notably in

the case of all-oxide solar cells [9]. In addition, a little asymmetry between the I-V curves obtained in the forward and reverse bias regions is observed. This behavior has already been observed in the literature [27] and was attributed to a modification of the charge carrier transport at the semiconductor/metal interface. Moreover, it is possible to calculate the ideality factor η[25,28] of this diode by measuring the slope in the linear region of the I-V characteristic, by using the relation $\eta = \frac{q}{kT}\frac{dV}{dLnI}$, where q is the electronic charge, k the Boltzmann constant, and T the temperature. We obtain an ideality factor equal to 16.8, thus far from 1. This value suggests the presence of interface layers between the $La_2Ti_2O_7$ thin film and the electrodes and the presence of conduction mechanism other than pure thermionic emission. Indeed, it is well known that the charge carrier transport in semiconductor materials can be modeled by several mechanisms [29] as Ohmic conduction, tunneling effect (Fowler-Nordheim) [30], Poole-Frenkel emission [30] or Space-Charge-Limited-Conduction (SCLC) [30]. The latter is commonly observed in the case of oxide materials when a high electric field is applied. In this case, the current density is proportional to the applied voltage by using the Mott-Gurney law [12], $j = \frac{9}{8}\mu\varepsilon_r\varepsilon_0\frac{V^2}{L^3}$ where μ is the charge carrier mobility, ε_0 is the vacuum permittivity, ε_r is the relative dielectric constant of sample and L is the distance between the electrodes. In order to precise the nature of the conduction mechanism, we represented on Figure 5 b, the evolution of the current density versus the applied voltage in a log-log diagram. We can note the presence of two regions: the first, for low field (i.e. $V < V_{tr}$=0.6 V), where the slope of the curve is close to 1. For this case, we can assume that the transport mechanism can be described by the Ohm law. The injection of charge carriers from the electrodes into the semiconductor material is strongly reduced due to the low bias voltage. Concerning the second region, for a high field (i.e. $V > V_{tr}$=0.6 V), we can observe a slope close

to 2, suggesting that the transport mechanism in this region can be described by the SCLC. This regime appears when the equilibrium charge concentration is less than the injected charge concentration. It is worth to remark that the same evolution of conduction mechanism was already observed in other oxide materials as CeO_x or TiO_x [29].We can conclude that there is two types of charge carrier conduction mechanism in the $La_2Ti_2O_7$ thin film, an Ohmic mechanism at low field and a SCLC mechanism at high field.

The time of flight method is a powerful experimental technic which allows the determination of the charge carrier mobility induced by light. Indeed, laser pulses focused on the sample (Figure 6) induce photo-charges in the sample.

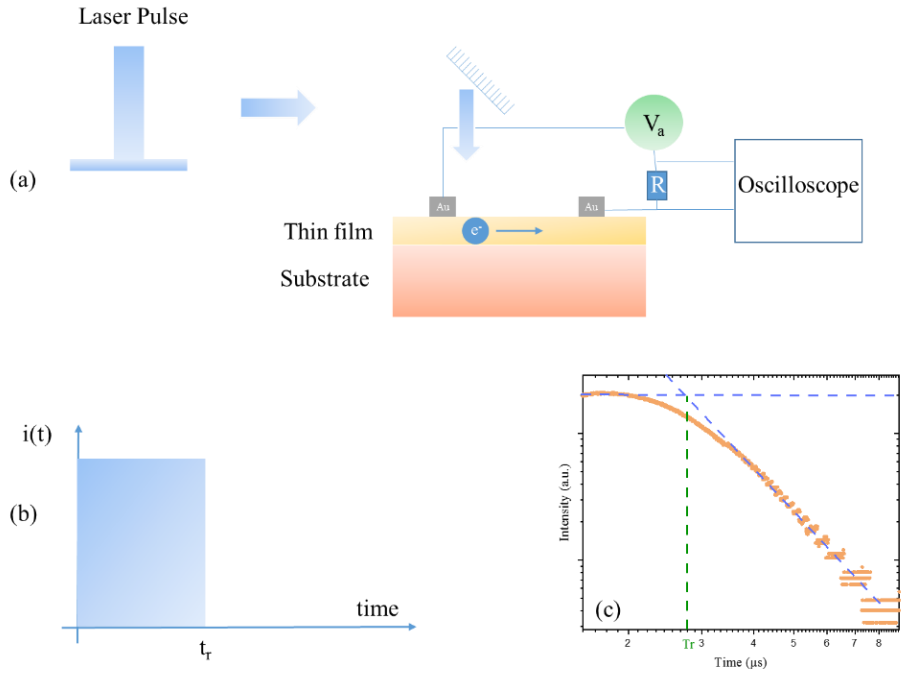

Figure 6. a) General description of time of flight experiment. b) Ideal photocurrent curve measured with TOF setup. c) Example of experimental time of flight curve.

The application of an electric field between two top electrodes induces a photocurrent. All recombined or captured charges are not able to reach the second electrode and do not contribute more to the photocurrent. The applied voltage can also sometimes play a harmful role in some cases, when we are in the presence of a Schottky contact[31], therefore in the presence of a diode with depletion layer, which can limit the mobility of the charges. Furthermore, it is commonly established that in the perovskites series the charge transport is dual, i.e. on the one hand electronic, and on the other ionic[16]. The time of flight setup using a nanosecond pulsed laser allows us to make the approximation that the mobility observed is only electronic. An electronic setup connected to these electrodes permits the measurement of the intensity of this photocurrent with time. The measurement of this drift time T_r allows the determination of the charge carrier mobility μ and their velocity v using the following relation.

$$\mu = \frac{L^2}{V_a T_r} \; ; \; v = \mu E = \frac{L}{T_r} \qquad (1)$$

Where L, E and V_a represent respectively the distance between gold electrodes, the applied electric field and the applied voltage.

In an ideal situation (Figure 6 b), the photocurrent i(t) is constant with time and drops to zero when all carriers are received by the collecting electrode for a time equal to the drift time T_r. During experimental measurements, we notice that the slope of i(t) is not constant as shown in Figure 6 c, but exhibits a cusp. The time at which the cusp appears corresponds to a moment when the majority of photo-generated carriers reach the collecting electrode and is considered as charge carrier transit time (T_r).

During this experiment, we recorded the photocurrent curves when varying several parameters as the laser power (7.5 mW, 12,5 mW and 20 mW) and the applied voltage (4V, 8V, 12 V, 16 V and

20 V). Table 1 gives the charge velocity and the charge mobility for experiments performed with an electrode gap fixed at 220 µm.

Laser power	Velocity ($m.s^{-1}$)					Mobility ($cm^2.V^{-1}.s^{-1}$)				
	4V	8V	12V	16V	20V	4V	8V	12V	16V	20V
7.5 mW	57.5	60.2	75.3	78.2	82.3	31.6	16.5	13.8	10.7	9.06
12.5 mW	67.4	65.8	67.9	77.1	78.0	37.1	18.1	12.4	10.6	8.58
20 mW	78.8	82.0	86.9	88.0	86.9	43.3	22.5	15.9	12.1	9.56

Table 1. Velocity and mobility of charge carriers measured on laser ablated $La_2Ti_2O_7$ thin film deposited on $SrTiO_3$ substrate with different applied voltages and laser powers.

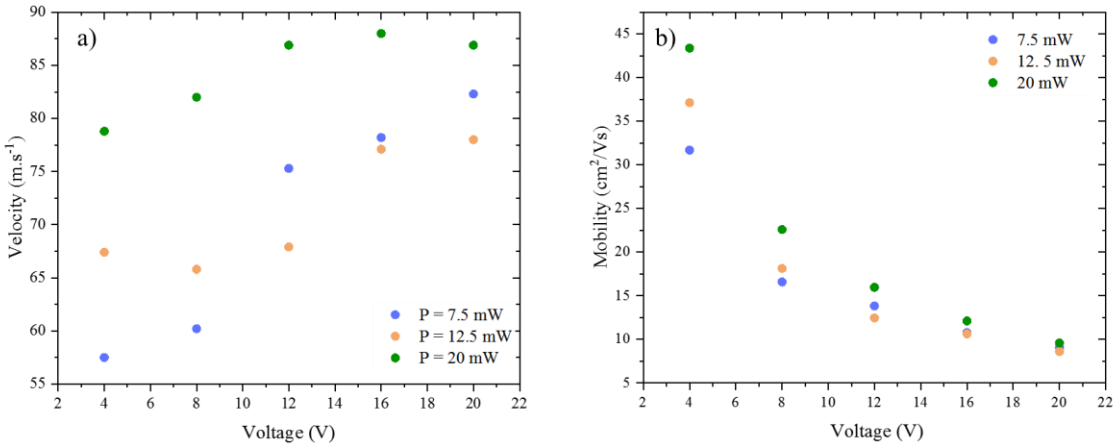

Figure 7. Evolution of velocity (a) and mobility (b) of electrons on $La_2Ti_2O_7$ thin film deposited on $SrTiO_3$ substrate with the applied voltage for three laser powers (7.5 mW, 12.5 mW and 20 mW)

The velocity of charge carriers versus the applied voltage is represented on Figure 7 a. One can note an increase of the charge carriers velocity with the applied voltage, but this evolution is not linear as expected from equation 1. Moreover, we observe a saturation of the velocity for the experiments performed with the highest laser power (20 mW).

Unexpectedly, a decrease of the mobility with the applied voltage is observed whatever the values of the laser power (figure 7.b). The same evolution was observed by Aduda *et al*. [31] in the case of TiO_2 thin films. On the other hand, the values of mobility are close to those measured on other oxides, but higher than $SrTiO_3$ (lower than 12 cm^2/Vs at room temperature)[32] but lower than ZnO (μ=180 cm^2/Vs at room temperature)[32]. Usually the evolution of the mobility with the applied voltage can be modeled by the Poole-Frenkel model in the case of metal-insulator-metal structure[33]. In this model, the mobility depends of the electric field by the following relation:

$$Ln(\mu) \propto E^{\frac{1}{2}} \qquad (2)$$

But, in our case, as observed previously, the junction between Gold contact and $La_2Ti_2O_7$ thin film do not play the role of an ohmic contact but must be represented by a Schottky junction. Actually, the work function (ϕ) of $La_2Ti_2O_7$ and Gold are w.r.t. vacuum level ϕ_{LTO} =4.45 eV [34] and ϕ_{Au} = 5.1 eV [35] and taking into account the n-semiconductor nature of $La_2Ti_2O_7$, we can easily assume that this junction can be modeled by a Schottky behavior as illustrated on Figure 8.

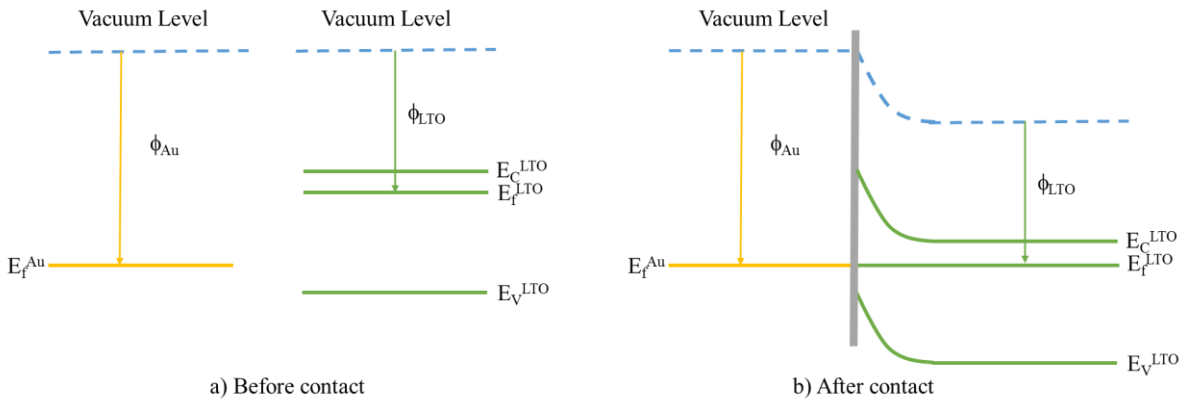

Figure 8. Schematic diagrams of energy band structure of the Au/$La_2Ti_2O_7$ junction before contact (a) and after contact (b)**.** ϕ_{Au} and ϕ_{LTO} correspond to the work function of Gold and $La_2Ti_2O_7$; E_f^{Au} and E_f^{LTO} correspond to the Fermi Level of Gold and $La_2Ti_2O_7$; E_v^{LTO} and E_c^{LTO} correspond to the energy of valence band and conduction band of $La_2Ti_2O_7$.

Furthermore, we can try to explain the negative dependence of the mobility with the electric field by using the model developed by Takashima[36]. In this model we firstly assume a heterogeneous electric field inside the thin film as the depletion layer created at the interface is subjected to an electric field E_d and the rest of the sample is subjected to the electric field E_b. E_d and E_b are depending on the applied voltage V_a, the length of the depletion area d and the distance between electrodes L using the following relation.

$$V_a = E_b(L - d) + E_d d \quad (3)$$

Secondly, we assume the conservation of the current density inside the depletion and bulk layers.

$$j_b = j_d = \sigma_b E_b = \sigma_d E_d \quad (4)$$

σ_b and σ_d represent the conductivity inside the bulk and depletion layers respectively

Using the two last relations we can define the electric field on the depletion and bulk layers with the following relations:

$$E_d = \frac{\sigma_b V_a}{[\sigma_b d + \sigma_d (L - d)]} \text{ and } E_b = \frac{\sigma_d V_a}{[\sigma_b d + \sigma_d (L - d)]} \quad (5)$$

Finally, we have defined the time of flight T_r between the two electrodes by the sum of the time of flight in the bulk layer T_b and the depletion layer T_d.

$$T_d = \frac{d}{\mu E_d} \text{ and } T_b = \frac{(L - d)}{\mu E_b} \quad (6)$$

$$T_r = T_d + T_b = \frac{d^2 + (\frac{\sigma_d}{\sigma_b} + \frac{\sigma_b}{\sigma_d})(L - d)d + (L - d)^2}{\mu V_a} \quad (7)$$

If we reasonably assume that the depth of the depletion layer is negligible compared to the distance between electrodes and that the conductivity in the depletion layer is lower than the conductivity in the bulk[37] we obtain the following approximation for the drift time of charge carriers between electrodes:

$$T_r = T_d + T_b = \frac{L^2 (1 + \frac{d}{L}\frac{\sigma_b}{\sigma_d})}{\mu V_a} \quad (8)$$

One can remark that this relation is similar to eq. (1) except the numerical factor which includes the characteristics of the depletion layer. We can include it on an effective applied voltage V_a^{eff}, $V_a^{eff} = \frac{V_a}{1 + \frac{d}{L}\frac{\sigma_b}{\sigma_d}}$. This relation allows to observe the decrease of the real applied voltage

compared to this which is experimentally controlled. Moreover, the length of the depletion layer can be determined by the following relation [37] :

$$d = \left(\frac{2\varepsilon_r \varepsilon_0}{eN_a}(V_a - V)\right)^{0.5} \quad (9)$$

V represents the height of the Schottky barrier, ε_r is the relative dielectric constant of $La_2Ti_2O_7$ and N_a the density of charge. One can note that the length of the depletion layer is depending on the applied voltage and can influence directly the mobility of the charge carriers during the measurement.

Assuming that V_a>V, we obtain the following relation:

$$T_r V_a = \psi V_a^{1/2} + \frac{L^2}{\mu} \quad (10)$$

Where, Ψ is a constant equal to $\frac{\sigma_b L}{\sigma_d}\left(\frac{2\varepsilon\varepsilon_0}{eN_a}\right)^{1/2}$. We plotted on Figure 9 the evolution of the product of the applied voltage and the drift time versus the square root of the applied voltage in the case of a thin film of $La_2Ti_2O_7$ for three laser powers. We noticed that the experimental points followed the linear trend of the equation 10. This allows us to conclude that the model developed by Takashima *et al*. [37]permits to explain correctly our measurement of drift time obtained for a thin film of $La_2Ti_2O_7$ and that this behavior is related to the dielectric properties of the Schottky barrier between the $La_2Ti_2O_7$ and the gold electrodes.

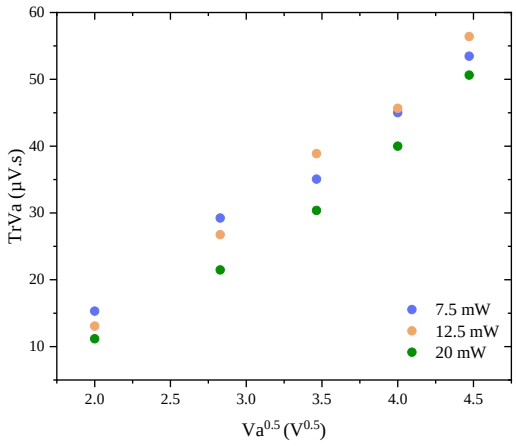

Figure 9. Evolution of the product of drift time by the applied voltage with the square root of the applied voltage for a $La_2Ti_2O_7$ thin film deposited on a $SrTiO_3$ substrate for three laser powers (7.5 mW, 12.5 mW and 20 mW)

Furthermore, we measured the evolution of the photocurrent versus the applied voltage between the gold electrodes. For this study, we represent the evolution of the maximum recorded value of the photocurrent versus the applied voltage for a laser power adjusted at 20 mW on Figure 10 a.

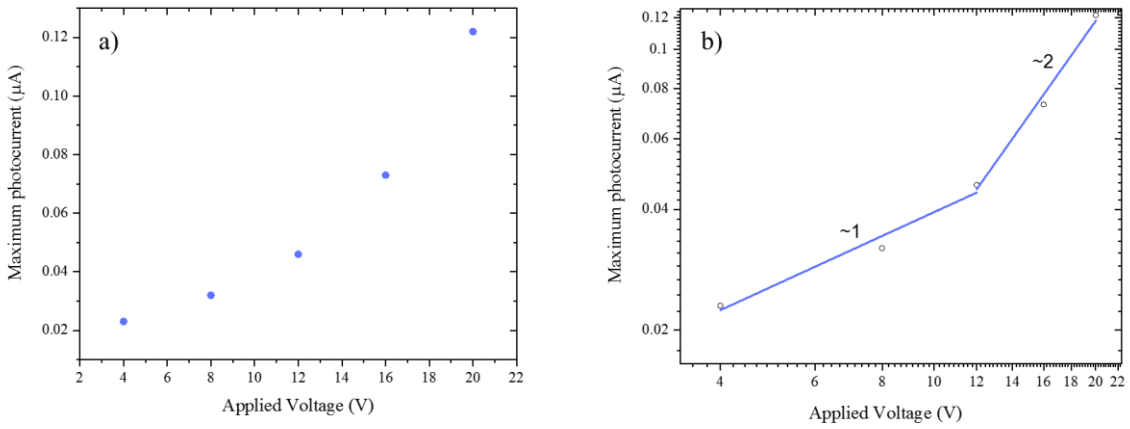

Figure 10. a) Evolution of maximum detected photocurrent with the applied voltage for a $La_2Ti_2O_7$ thin film deposited on a $SrTiO_3$ substrate and a laser power fixed at 20 mW b) Evolution of maximum detected photocurrent with the applied voltage for a $La_2Ti_2O_7$ thin film deposited on a $SrTiO_3$ substrate and a laser power fixed at 20 mW in log-log diagram.

The curve seems to follow a quadratic dependence with the applied voltage as for example, the Mott-Gurney law [12] $j = \frac{9}{8}\mu\varepsilon_r\varepsilon_0\frac{V^2}{L^3}$, but in our study this relation cannot fit exactly with the experimental curve on the whole range. Indeed, as presented previously on the I-V characteristics, it is usually assumed that conductivity at low field regime follows the Ohm law and that the high field region can be governed by a Space-Charge-Limited-Conduction mechanism [38] and we guess that the photocurrent can follow the same evolution. To check the presence of these two regimes, we represented the latter graph in double logarithm plot on Figure 10 b. Despite a small number of experimental points, one can notice as expected, the presence of two regimes. The first, at low voltage (between 4 V and 13 V) exhibits a linear tendency with a slope approximatively equal to 1; we can conclude that this region can be governed by the Ohm law. The second regime (above 13 V) exhibits a linear tendency with a slope approximatively equal to 2; in this region, we can conclude that the photoconduction mechanism can be leaded by a transient Space-Charge Limited Current model. In addition, we can note a good correlation between the I-V characteristics presented in Figure 5 b and the I-V curve extracted from TOF measurements presented in Figure 10 b. Nevertheless, we cannot compare directly these values. Indeed, we can note the difference between the voltage thresholds which are 0.6 V and 12 V in the two experiments, respectively. This difference can be easily explained by i) The difference of distance between the electrodes: the voltage was applied across the film (390 nm of thickness) in

the I-V measurements and was applied in a lateral configuration in the TOF measurements (220 µm between the two electrodes). ii) The difference of crystallographic structure which can affect the charge carrier mobility: the LTO film possess a polycrystalline structure in the case of I-V measurements and an epitaxial structure in the case of TOF measurements. These two factors can affect directly the measurements and we can only qualitatively compare the samples.

CONCLUSION

We deposited $La_2Ti_2O_7$ thin films on two substrates, Silicon covered by a Platinum layer on one side and $SrTiO_3$ on the other side. The structural characterizations were performed by XRD and spectroscopic ellipsometry. We showed that the thin films have polycrystalline orientation when they are deposited on Pt-(111)/TiO_x/Si substrate and have (012) and (025) orientations with respect to the plane of the substrate when the film are deposited on (100)-oriented $SrTiO_3$ substrate. The sample deposited on the Silicon substrate was used to obtain the I-V curves in dark and under UV illumination. We note an increase of the current when the sample is illuminated by the UV light and the presence of two conduction regimes: Ohmic at low electric field and a SCLC mechanism at high electric field. In addition, we report for the first time at our knowledge the measurement of the carrier mobility of $La_2Ti_2O_7$ thin films by the Time of Flight method. The electronic mobility was estimated around 30 $cm^2.V^{-1}.s^{-1}$ and we note as shown previously for the I-V curves two electronic conduction regimes.

EXPERIMENTAL SECTION

Dititanate lanthanum oxide target was synthesized using a standard solid-state reaction route. La_2O_3 (99.9% STREM CHEMICAL) and TiO_2 (99.9% GERAC) were used as starting materials. Note that as La_2O_3 oxide is highly hygroscopic, it must undergo a thermal pre-treatment at 800°C to obtain the correct stoichiometry. After this pre-treatment, a stoichiometric mixture of precursors is grinded in ethanol during 20 min. Then, the ground powders are packed in alumina crucible and calcined, under air, at 1100°C during 12 hours (grinding and calcination steps are repeated two times to enhance sample homogeneity). Then, the powders are re-ground, and then placed in the uniaxial press to generate PLD targets (1-inch diameter). Finally, these pellets are sintered at 1400°C during 12h. X-Ray diffraction measurements, realized on the pellets, confirm the presence of the expected $La_2Ti_2O_7$ with monoclinic structure ($P2_1$), with no impurity.

Thin films were afterward grown by Pulsed Laser Deposition (PLD) using a Compex Pro 102 laser (KrF excimer laser operating at a wavelength of 248 nm). The laser frequency is adjusted at a rate of 3 Hz with an energy density of 2 J/cm^2 and the target-substrate distance fixed at d= 4.5 cm. The number of laser pulses was adjusted at 10000 for the thin film deposited on $SrTiO_3$ substrate and 15000 for the thin film deposited on $Pt/TiO_x/Si$ substrate.

Top gold electrodes were deposited on the LTO thin films using vacuum evaporation technique. The LTO thin films samples were overlaid by a mask, which presents several stampings, with different shapes and sizes. Both samples and mask were disposed on a sample rack, and pinched with clamps. The thickness of the gold deposit was constantly measured, so it was possible to stop the deposit when the wanted thickness was reached

The structural characterization of the films was performed using a Rigaku SmartLab high resolution X-rays diffractometer equipped with a 9 kW rotating anode X-ray generator ($\lambda K\alpha_1$ = 1.54059 Å). The X-Ray beam was made parallel with cross-beam optics and monochromatized

with a double Ge (220) monochromator. In this study all the (ω-2θ) scans were performed in the range of 10° - 80°, with a step size of 0.01° and a speed of 3°/min. μXRD measurement was done using CBO-f optics, providing a 400 μm beam spot size. An offset of 2° relative to the substrate was applied in order to measure only the deposited film.

Spectroscopic Ellipsometry measurements were performed at room temperature using a phase-modulated ellipsometer (UVISEL HR460 from Horiba Scientific) at wavelengths ranging from 260 to 1500 nm with 2 nm interval. An incidence angle of 70° was used for all measurements. The raw signal measured by Spectroscopic Ellipsometry has the following structure: $I(t) = I_0 + I_S \sin(\delta(t)) + I_C \cos(\delta(t))$, where δ(t) is the time dependent phase shift of a modulator. In our experimental configuration, the value of I_0, I_C and I_S are linked to the ellipsometric angles (Δ, Ψ) by the following relations: $I_0 = 1$, $I_S = \sin 2\Psi \sin \Delta$, $I_C = \sin 2\Psi \cos \Delta$. The ellipsometric angles Δ and Ψ are related to the complex reflection coefficients of polarized light (R_p and R_s for respectively a polarization parallel and perpendicular to the plane of incidence) by the following relation $\rho = \frac{R_P}{R_S} = \tan \psi e^{i\Delta}$. For each sample, the measured spectra may be analyzed using an appropriate fitting model based on sample structure. Data fitting were performed using the Delta-Psi Horiba software.

Voltage-current measurements were performed by using a Keysight B2902A precision source/measure unit; the setup is equipped with metallic probes mounted on a micrometer positioning stage to ensure a good contact on top electrodes deposited on the sample. The probes are also used for polarization measurements and time of flight experiments.

Time of flight experiments were carried on with a Nd:YAG laser (λ= 355nm, pulse width= 5 ns). The photogenerated charge carriers are moved by applying a bias using a Keithley 6487 voltage

source. The resulting transient photocurrent curves were recorded using a shunt resistor of 1 kΩ, a low-noise preamplifier (Stanford Research, SR 560) and a digital oscilloscope (Keysight DSO-X3022T).

SUPPORTING INFORMATION

Figure S1. Rocking-curves performed for φ=0° et φ=45° on (012) reflection of $La_2Ti_2O_7$ and sketch illustrating the existence of four domains in $La_2Ti_2O_7$ thin film grown on (100)-oriented $SrTiO_3$ substrate.

Figure S2. a) Structure of $La_2Ti_2O_7$ and angle between (012) and (025) planes; b) Scheme highlighted the adaptation of $La_2Ti_2O_7$ on a (100)-$SrTiO_3$ substrate.

AUTHOR INFORMATION

Corresponding Author

Pr. Jean-François Blach,

*Université d'Artois, Unité de Catalyse et de Chimie du Solide, UCCS,

Équipe couches minces et nanomatériaux, CNRS-UMR 8181, Faculté des Sciences Jean Perrin,

F-62300 LENS, France

Phone: +33 321791752, Fax: +33 321177955, E-mail: jfrancois.blach@univ-artois.fr

ACKNOWLEDGMENT

Chevreul Institute (FR 2638)", "Ministère de l'Enseignement Supérieur et de la Recherche", "Région Hauts-de-France", "FEDER" and "C'Nano Nord-Ouest compétence centre" are acknowledged for supporting and funding this work.

References

(1) Thery, V.; Bayart, A.; Blach, J. F.; Roussel, P.; Saitzek, S. Effective Piezoelectric Coefficient Measurement of $BaTiO_3$ Thin Films Using the X-Ray Diffraction Technique under Electric Field Available in a Standard Laboratory. *Appl. Surf. Sci.* **2015**, *351*, 480–486. https://doi.org/10.1016/j.apsusc.2015.05.155.

(2) Yang, S. Y.; Martin, L. W.; Byrnes, S. J.; Conry, T. E.; Basu, S. R.; Paran, D.; Reichertz, L.; Ihlefeld, J.; Adamo, C.; Melville, A.; Chu, Y. H.; Yang, C. H.; Musfeldt, J. L.; Schlom, D. G.; Ager, J. W.; Ramesh, R. Photovoltaic Effects in $BiFeO_3$. *Appl. Phys. Lett.* **2009**, *95* (6), 25–27. https://doi.org/10.1063/1.3204695.

(3) Larcher, D.; Delobel, B.; Dantras-Laffont, L.; Simon, E.; Blach, J.-F.; Baudrin, E. Formation of Nanometric HT-$LiCoO_2$ by a Precipitation and Aging Process in an Alcoholic Solution. *Inorg. Chem.* **2010**, *49* (23), 10949–10955. https://doi.org/10.1021/ic101324e.

(4) Bayart, A.; Katelnikovas, A.; Blach, J.; Rousseau, J.; Saitzek, S. Synthesis, Structural and Luminescence Properties of $(La_{1-x}Ln_x)_2Ti_2O_7$ (Ln=lanthanides) Solid Solutions. *J. Alloys Compd.* **2016**, *683*, 634–646. https://doi.org/10.1016/j.jallcom.2016.05.041.

(5) Atuchin, V. V.; Gavrilova, T. A.; Grivel, J. C.; Kesler, V. G. Electronic Structure of Layered Ferroelectric High-k Titanate $La_2Ti_2O_7$. *J. Phys. D. Appl. Phys.* **2009**, *42* (3). https://doi.org/10.1088/0022-3727/42/3/035305.

(6) Nashim, A.; Martha, S.; Parida, K. M. Heterojunction Conception of N-$La_2Ti_2O_7$/p-CuO in

the Limelight of Photocatalytic Formation of Hydrogen under Visible Light. *RSC Adv.* **2014**, *4* (28), 14633. https://doi.org/10.1039/c3ra47037g.

(7) Nashim, A.; Parida, K. M. Novel $Sm_2Ti_2O_7/SmCrO_3$ Heterojunction Based Composite Photocatalyst for Degradation of Rhodamine 6G Dye. *Chem. Eng. J.* **2013**, *215–216*, 608–615. https://doi.org/10.1016/j.cej.2012.11.025.

(8) Nashim, A.; Pany, S.; Parida, K. M.; Nanda, J. $La_2Ti_2O_7$ As Nanometric Electrode Material: An Emerging Candidate For Supercapacitor Performance. *ChemistrySelect* **2019**, *4* (41), 12037–12042. https://doi.org/10.1002/slct.201903227.

(9) Rühle, S.; Anderson, A. Y.; Barad, H.; Kupfer, B.; Bouhadana, Y.; Rosh-Hodesh, E.; Zaban, A. All-Oxide Photovoltaics. *J. Phys. Chem. Lett.* **2012**, *3* (24), 3755–3764. https://doi.org/10.1021/jz3017039.

(10) Xiao, H. Y. Electronic Structure Calculations of $A_2Ti_2O_7$ (A = Dy, Ho, and Y). *Adv. Condens. Matter Phys.* **2013**, *2013*, 1–8. https://doi.org/10.1155/2013/675410.

(11) Sayede, a.; Khenata, R.; Chahed, a.; Benhelal, O. Electronic and Optical Properties of Layered $RE_2Ti_2O_7$ (RE = Ce and Pr) from First Principles. *J. Appl. Phys.* **2013**, *113* (17), 173501. https://doi.org/10.1063/1.4803124.

(12) Röhr, J. A.; Shi, X.; Haque, S. A.; Kirchartz, T.; Nelson, J. Charge Transport in Spiro-OMeTAD Investigated through Space-Charge-Limited Current Measurements. *Phys. Rev. Appl.* **2018**, *9* (4). https://doi.org/10.1103/PhysRevApplied.9.044017.

(13) Reid, O. G.; Munechika, K.; Ginger, D. S. Space Charge Limited Current Measurements on Conjugated Polymer Films Using Conductive Atomic Force Microscopy. *Nano Lett.*

2008, *8* (6), 1602–1609. https://doi.org/10.1021/nl080155l.

(14) Li, H.; Duan, L.; Zhang, D.; Dong, G.; Qiao, J.; Wang, L.; Qiu, Y. Relationship between Mobilities from Time-of-Flight and Dark-Injection Space-Charge-Limited Current Measurements for Organic Semiconductors: A Monte Carlo Study. *J. Phys. Chem. C* **2014**, *118* (12), 6052–6058. https://doi.org/10.1021/jp411948d.

(15) Pavlica, E.; Bratina, G. Time-of-Flight Mobility of Charge Carriers in Position-Dependent Electric Field between Coplanar Electrodes. *Appl. Phys. Lett.* **2012**, *101* (9), 093304. https://doi.org/10.1063/1.4742149.

(16) Emin, S.; Pavlica, E.; Okuyucu, H.; Valant, M.; Bratina, G. Charge Carrier Transport in Polycrystalline $CH_3NH_3PbI_3$ Perovskite Thin Films in a Lateral Direction Characterized by Time-of-Flight Photoconductivity. *Mater. Chem. Phys.* **2018**, *220* (January), 182–189. https://doi.org/10.1016/j.matchemphys.2018.08.012.

(17) Prashanthan, K.; Thivakarasarma, T.; Balashankar, K.; Ravirajan, P. Effect of Interface Modifiers on Hole Mobility in Hybrid Nanoporous Titanium Dioxide (TiO_2) / Poly(3-Hexylthiophene) (P3HT) Solar Cells. *IEEE-NANO 2015 - 15th Int. Conf. Nanotechnol.* **2015**, No. October 2017, 736–738. https://doi.org/10.1109/NANO.2015.7388713.

(18) Shao, Z.; Saitzek, S.; Roussel, P.; Ferri, A.; Mentré, O.; Desfeux, R. Investigation of Microstructure in Ferroelectric Lead-Free $La_2Ti_2O_7$ Thin Film Grown on (001)-SrTiO3 Substrate. *CrystEngComm* **2012**, *14* (20), 6524. https://doi.org/10.1039/c2ce26078f.

(19) Ohtomo, A.; Muller, D. A.; Grazul, J. L.; Hwang, H. Y. Epitaxial Growth and Electronic Structure of $LaTiO_x$ Films. *Appl. Phys. Lett.* **2002**, *80* (21), 3922–3924.

https://doi.org/10.1063/1.1481767.

(20) Shibuya, K.; Ohnishi, T.; Kawasaki, M.; Koinuma, H.; Lippmaa, M. Metallic $LaTiO_3$/ $SrTiO_3$ Superlattice Films on the $SrTiO_3$(100) Surface. *Jpn. J. Appl. Phys.* **2004**, *43* (No. 9A/B), L1178--L1180. https://doi.org/10.1143/jjap.43.l1178.

(21) Schmalle, H. W.; Williams, T.; Reller, A.; Linden, A.; Bednorz, J. G. The Twin Structure of $La_2Ti_2O_7$: X- ray and Transmission Electron Microscopy Studies. *Acta Crystallogr. Sect. B* **1993**, *49* (2), 235–244. https://doi.org/10.1107/S010876819200987X.

(22) Bayart, A.; Saitzek, S.; Chambrier, M. H.; Shao, Z.; Ferri, A.; Huvé, M.; Pouhet, R.; Tebano, A.; Roussel, P.; Desfeux, R. Microstructural Investigations and Nanoscale Ferroelectric Properties in Lead-Free $Nd_2Ti_2O_7$ Thin Films Grown on $SrTiO_3$ Substrates by Pulsed Laser Deposition. *CrystEngComm* **2013**, *15* (21), 4341–4350. https://doi.org/10.1039/c3ce40256h.

(23) Salzmann, I.; Resel, R. STEREOPOLE: Software for the Analysis of X-Ray Diffraction Pole Figures with IDL. *J. Appl. Crystallogr.* **2004**, *37* (6), 1029–1033. https://doi.org/10.1107/S002188980402165X.

(24) Bayart, A.; Blach, J. F.; Huvé, M.; Blanchard, F.; Roussel, P.; Desfeux, R.; Saitzek, S. Optical Properties of $Ln_2Ti_2O_7$ (with Ln = La to Lu)Thin Films Grown on (110)-$SrTiO_3$ Substrates by Pulsed Laser Deposition. *Opt. Mater. (Amst).* **2019**, *92* (February), 303–310. https://doi.org/10.1016/j.optmat.2019.04.049.

(25) Rajan, L.; Periasamy, C.; Sahula, V. Electrical Characterization of Au / ZnO Thin Film Schottky Diode on Silicon Substrate. *Perspect. Sci.* **2016**, *8*, 66–68.

https://doi.org/10.1016/j.pisc.2016.03.011.

(26) Borkar, H.; Rao, V.; Tomar, M.; Gupta, V.; Scott, J. F.; Kumar, A. Giant Enhancement in Ferroelectric Polarization under Illumination. *Mater. Today Commun.* **2018**, *14* (November 2017), 116–123. https://doi.org/10.1016/j.mtcomm.2017.12.004.

(27) Ma, Z.; Li, L.; Wang, Y.; Zhou, P.; Guo, Y.; Liu, Y.; Liang, K.; Qi, Y.; Zhang, T. Write Voltage-Dependent Transport Mechanisms in Pt/$BaTiO_3$ /Nb:$SrTiO_3$ Ferroelectric Tunnel Memristors. *Appl. Phys. Lett.* **2020**, *116* (3), 032903. https://doi.org/10.1063/1.5141903.

(28) Cheung, S. K.; Cheung, N. W. Extraction of Schottky Diode Parameters from Forward Current-Voltage Characteristics. *Appl. Phys. Lett.* **1986**, *49* (2), 85–87. https://doi.org/10.1063/1.97359.

(29) Lim, E. W.; Ismail, R. Conduction Mechanism of Valence Change Resistive Switching Memory: A Survey. *Electron.* **2015**, *4* (3), 586–613. https://doi.org/10.3390/electronics4030586.

(30) Chiu, F. A Review on Conduction Mechanisms in Dielectric Films. *Adv. Mater. Sci. Eng.* **2014**, *2014* (Article ID 578168).

(31) Aduda, B. O.; Ravirajan, P.; Choy, K. L.; Nelson, J. Effect of Morphology on Electron Drift Mobility in Porous TiO_2. *Int. J. Photoenergy* **2004**, *6* (3), 141–147. https://doi.org/10.1155/S1110662X04000170.

(32) Trier, F.; Christensen, D. V.; Pryds, N. Electron Mobility in Oxide Heterostructures. *J. Phys. D. Appl. Phys.* **2018**, *51* (29). https://doi.org/10.1088/1361-6463/aac9aa.

(33) Schroeder, H. Poole-Frenkel-Effect as Dominating Current Mechanism in Thin Oxide Films—An Illusion?! *J. Appl. Phys.* **2015**, *117* (21), 215103. https://doi.org/10.1063/1.4921949.

(34) Nashim, A.; Parida, K. N-$La_2Ti_2O_7$ / p-$LaCrO_3$: A Novel Heterojunction Based Composite Photocatalyst with Enhanced Photoactivity Towards ... *J. Mater. Chem. A Mater. energy Sustain.* **2014**, *2* (October), 18405–18412. https://doi.org/10.1039/C4TA02401J.

(35) Lin, Y. B.; Yan, Z. B.; Lu, X. B.; Lu, Z. X.; Zeng, M.; Chen, Y.; Gao, X. S.; Wan, J. G.; Dai, J. Y.; Liu, J. M. Temperature-Dependent and Polarization-Tuned Resistive Switching in Au/$BiFeO_3$/$SrRuO_3$ Junctions. *Appl. Phys. Lett.* **2014**, *104* (14). https://doi.org/10.1063/1.4870813.

(36) Takashima, H.; Shimada, K.; Miura, N.; Katsumata, T.; Inaguma, Y.; Ueda, K.; Itoh, M. Low-Driving-Voltage Electroluminescence in Perovskite Films. *Adv. Mater.* **2009**, *21* (36), 3699–3702. https://doi.org/10.1002/adma.200900524.

(37) Takashima, W.; Pandey, S. S.; Endo, T.; Rikukawa, M. Effects of Regioregularity on Carrier Transport in Poly(Alkylthiophene) Films with Various Alkyl Chain Lengths. *Curr. Appl. Phys.* **2001**, *1*, 90–97.

(38) Lebedev, A.; Dittrich, T. Space Charge Limited Current in Porous Silicon and Anatase (TiO_2). *Semiconductors* **2002**, *36* (10), 1188–1191. https://doi.org/10.1134/1.1513867.